Energy Conversion and Management 157 (2018) 215–223

Contents lists available at ScienceDirect

Energy Conversion and Management

journal homepage: www.elsevier.com/locate/enconman

Thermoelectric energy harvesting for the gas turbine sensing and monitoring system

Yongjia Wu[a], Haifeng Zhang[b], Lei Zuo[a,*]

[a] Energy Harvesting and Mechatronics Research Lab, Department of Mechanical Engineering, Virginia Tech, Blacksburg, VA 24060, United States
[b] Department of Mechanical and Energy Engineering, University of North Texas, Denton, TX 76210, United States

ARTICLE INFO

Keywords:
Thermoelectric
Gas turbine
Sensing and monitoring
Power generation

ABSTRACT

A compact thermoelectric energy harvester is developed to harvest the thermal energy from the hot surface of the gas turbine, providing continuous and reliable power for the sensing and monitoring system in the gas turbine. An experimental prototype is built and the performances of the energy harvester with different electrical load resistances and source temperatures are characterized. A mathematical iterative method, taking account of Thompson Effect, line spacing gap heat leakage, material property variations, and thermal resistance of the ceramic covering layer, is used to analyze the performance of the segmented thermoelectric generator (TEG) module with good accuracy. Based on this model, the temperature profiles and heat fluxes along the thermo-elements, efficiency, and heat leakage through the filling gap material are analyzed. The prototype, with a source temperature of 325 °C, has a voltage output of 2.4 V and power output of 0.92 W, which is more than enough to power a sensor node in the gas turbine. A higher power output can be expected with some improvement on the prototype design.

1. Introduction

1.1. Thermoelectric energy harvesting

The TEG, using electrons (for N-type) and holes (for P-type) as the "working fluid", is an attractive energy harvesting technology to convert thermal energy to electricity without any moving components [1]. The efficiency of the TEG varies with the temperature difference and ZT value, typically ranging between 1 and 20% at the current state. The primary effort to improve the efficiency of TEG device was focused on improving the materials' figure-of-merit guiding by phonon and electron transmission theory [2,3]. Since the observation of Seebeck effect in 1821, the development of thermoelectric materials was quite slow till the discovery of semiconductors in the1950s. In 1993, Hicks and Dresselhaus [4,5] predicted that, taking advantage of the quantum effect, it was possible to achieve a ZT value higher than 10.0 in the low dimensional thermoelectric materials, including supper lattice, nanowire, and nanoparticles. This inspiring prediction significantly stimulated the research of nanostructured thermoelectric materials in the next decades. Since then, various materials with ZT values higher than 1.0 were found [6,7]. According to the newest research by Harman et al., the highest ZT reported was 3.5 in Bi-doped n-type PbSeTe/PbTe quantum-dot super-lattice [8]. Though low dimensional thermoelectric materials are theoretically predicted superior to bulk materials, fabrication of nanomaterials with stable and reliable performance can be challenging [9]. Besides nanomaterials, the highest ZT value of bulk thermoelectric material was reported to be as high as 2.6 ± 0.3 at 923 K in SnSe single crystals measured along the b axis of the orthorhombic unit cell [10]. To develop the third generation thermoelectric materials with high ZT values, researchers proposed several potential strategies, including band convergence [11,12], composition and microstructure manipulations [13], strained endotaxial nanostructuring [14], matrix/precipitate band alignment [15], and compositionally alloyed nanostructuring [16]. However, some researchers claimed that it was only when the ZT value of the commercial bulk thermoelectric material was higher than 3.0, would the TEG be able to compete with the conventional thermal engines [17]. Currently, the TEG is still restricted on relatively small scale, decentralized energy harvesting [18,19].

The system level thermal design should be equally important to achieve high performance [2,20]. To enhance the efficiency of the TEG, a large temperature difference should be sustained between the two ends of the thermo-elements. Conventionally, optimization-designed heat sinks/exchangers are mounted on the hot and cold ends of the TEG to maximize the temperature drop. For the high temperature range application, the segmented TEG, consisting of low-, medium- and high-

* Corresponding author.
E-mail address: leizuo@vt.edu (L. Zuo).

https://doi.org/10.1016/j.enconman.2017.12.009
Received 18 August 2017; Received in revised form 14 November 2017; Accepted 4 December 2017
Available online 18 December 2017
0196-8904/

Nomenclature

Symbols

RH	thermal resistance (K/W)
L	the length of the thermos-pellets (m)
k	thermal conductivity (W/(K m))
A	cross-section area (m^2)
ε	absorption coefficient
σ	Stefan-Boltzman constant
F	relative view factor
T	temperature (K)
q	heat flow (W/m^2)
α	seebeck coefficient (V/K)
I	current (A)
V	voltage (V)
R	electrical resistance (Ω)
N	the number of thermos-couple
ρ	electrical resistivity(Ω m)
P	power output (W)
J	electrical density (A/m^2)
x	coordinate position (m)

Subscript

$P1$,$P2$	P-type thermo-element near to the hot/cold side
$N1$,$N2$	N-type thermo-element near to the hot/cold side
H,C	Hot/Cold side
G	air filling gap
h,c	hot/cold side of the thermo-element
P,N	P/N-type thermos-pellet
Ph,Nh,Pc,Nc	hot/cold side of the P/N-type thermos-pellet
$m1$,$m2$	the intersection of the thermo-element segments
H,C	hot/cold side of the TEG module
L	load
M	module
i	coordinates

Abbreviations

TEG	thermoelectric generator
MEMS	microelectromechanical system

temperature thermoelectric materials, are combined to maximize the overall conversion efficiency of the thermo-element by taking full advantage of the characteristics of different thermoelectric materials [21,22]. When design segmented TEG, compatibility factor issue should be carefully handled [23].

TEG technology was heavily researched in the past decades, such as harvesting waste heat from the automobile exhaust to recharge the battery thus reducing the load on the engine [24–26]. In recent years, TEG applied to energy harvesting for wireless sensor nodes has attracted increasing attention [18,27,28]. The self-powered wireless sensor nodes can provide redundant and independent measurements of operation parameters for the nuclear power plant, bridges, high building, aircraft, gas turbine, etc. TEG energy harvesters with various size and power output were designed to meet the demand of different electrical devices [17,29–31]. Inspired by the Fukushima nuclear power plant accident, Clayton et al. [32] proposed the possibility to develop a wireless sensing and monitoring system based on TEG energy harvester in the nuclear power plant. Taking advantage of the ubiquitous pipes in the plant, the TEG can extract thermal energy from the hot pipe to power the system even during station blackout accidents. In the aerospace industry, composite material like glass fiber reinforced plastics and carbon fiber reinforced plastics are widely used to improve the aircraft efficiency. A network of sensors is distributed over the structural area of interest to monitor the material health. To power these sensors, a thermoelectric solution was introduced by Samson et al. [27] to harvest energy from the aerospace engine. Kousksoua et al. [33] investigated the electric power extractable from a helicopter conical nozzle equipped with TEG. They developed a numerical model to analyze the performance of the TEG energy harvester under different operating conditions. With an exhaust gas temperature of 900 K, the output power was more than 400 W. However, they did not do any experiment to examine their result. In Ref. [34], a wearable glass fabric-based flexible TEG fabricated by a screen printing technique was presented. The research aimed at harvesting energy from the human body to power the mobile devices and health monitoring sensors. Hudak and Amatucci [18] reviewed the recent progress in three different energy harvesting technologies for small-scale devices, including thermoelectric power generation, vibration-to-electric power conversion, and radiofrequency power conversion. In most situation, when compared with kinetic and radiated energies, the thermal energy that can be harvested has a higher energy density, making it extremely suitable for energy harvesting in an environment with thermal source available.

To minimize the impact of sensing and monitoring system on the performance of the operating device, the sensing and transmitting components continue to be scaled down along with the decrease in the energy consumption. To make the whole system compact and reliable, there is an urgent need to shrink the size of energy harvester. The “Smart Dust” project [35,36] supported by DARPA (The Defense Advanced Research Projects Agency) set an arbitrary goal of 1.0 mm^2 per node. With the development of MEMS techniques, including electrochemical MEMS, chemical vapor deposit (CVD), and sputtering, the thermo-element of TEG has been miniaturized to μm-scale, which can be easily embedded in various systems. In the work of Huesgen et al. [28], they fabricated a MEMS TEG with high integration density using thin-film processing technologies on the wafer surface. A novel thermal connector was designed to guide the heat flow to pass the thermo-elements perpendicular to the chip surface. Though losing some heat due to thermal shorting of the substrate, the device can benefit from the longer thermo-elements, having a higher voltage output. Substituting the wafer with a polyimide substrate, the device can be adapted to make a flexible μm-scale TEG, harvesting milli-watts energy with a small temperature difference to power a wristwatch [19,37]. The website of Thermo Life Energy Corporation reported an energy density of 40 μW/cm^2 and voltage output of 2.7 V at $\Delta T = 5$ K for a similar design [38].

To analyze and optimize the performance of TEG more accurately, the analytical models were more and more sophisticated [39–41], taking account of the radiation heat transfer, heat leakage, contact resistance, temperature-dependent material properties, and Thompson Effect. However, analytical solutions exist only for simple scenarios. In most situation, some reasonable assumptions were made to simplify the modeling. Numerical models are more widely used to simulate thermal systems with TEG integrated. Commercial finite element method (FEM) software, such as ANSYS and COMSOL, were widely used to do thermoelectric simulations [42,43]. Jang et al. [43] simulated a TEG waste energy harvesting system using the commercial ANSYS FLUENT software. Their simulation coupled the TEG with the well-validated turbulence flow models and the radiation models imbedded in the software. The simulation result matched very well with the experimental result. Ming et al. [22] studied a geometry-optimized segmented TEG module operating between 300 K and 780 K using commercial ANSYS package. Different heat flux conditions were tested, the segmented TEG model achieved a peak efficiency of 11.2%. For even complicated cases where TEG simulation coupled with heat and mass transfer processes,

semi-empirical relationships can be more accurate and easy-implemented than computational fluid dynamics (CFD) simulation [44,45].

1.2. Self-powered wireless sensors in the gas turbine

The gas turbine is a key component in a modern power plant, aircraft, and ship (Fig. 1(a)). The increasing complexity of gas turbine has led to the desired need to introducing the reliable, smart, and automated prognostic and health monitoring systems. To provide such capability, hundreds of sensors of varying types are embedded in the engine to collect various physical parameters, such as pressure, temperature, vibration, and gas chemical compositions associated with engine operation (Fig. 1(b)). Then, the data are transmitted to a central data processing unit, where the data are stored and processed. In the traditional wired sensing and monitoring system, cables of thousands of meters long are used to power the sensors and the auxiliary electronic devices. However, exposed to the harsh environment with high temperature and large vibrations, the expensive, long, and heavy cables make the overall system unreliable [32]. To solve these problems, there is a need to develop an energy-independent wireless system. The system, taking advantage of the energy source in the sensor environment, can supply reliable, stable, and independent electric power for the sensing and monitoring systems. In this paper, we develop a thermoelectric energy harvester to harvest the thermal energy from the gas turbine surface for the autonomous sensor nodes in the gas turbine, providing continuous, real-time, and reliable operation parameter sensing and monitoring for the data center (Fig. 1(b)).

To address this issue, there are several practical problems should be solved before it can be integrated into the existing system. For a modern gas turbine, the temperature in the combustion chamber can be as high as 1200 °C, which is a great challenge for the blade and chamber. To prolong the lifecycle of the system, a high-efficiency and sophisticated cooling system design [46] combined with the thermal barrier coatings technology [47] is adopted in the industrial gas-turbine engines. Before entering the combustion chamber, the air coming out from the compressor at a temperature nearly 300 °C flows through the cooling channels covering the combustion chamber, at the same time preheated by the combustion chamber wall. Unlike the common situation, the extreme working conditions, such as high temperature (> 300 °C), bring about extra complication to the energy harvester design. Meanwhile, the gas turbine for power generation is covered by a thick thermal isolation material layer to prevent heat leakage and sustain high efficiency. To efficiently use the temperature difference between the gas turbine surface and the ambient environment, the thermal network should be carefully designed. Meanwhile, to minimize the impact of sensing and monitoring system on the performance of the gas turbine, the energy harvester should be compact and shall not involve active cooling system. There is also a lack of experimental study of an energy harvester using segmented TEG to harvest thermal energy for the autonomous senor nodes.

For a sensor node working in transmission mode, the general energy consumption is about 50 mW [27]. In this paper, we build and test an segmented TEG energy harvester prototype with the hot end temperature reaching up to 325 °C for the gas turbine sensor system. The TEG energy harvester developed here can harvest ~0.92 W energy, which is more than enough for the sensor node and auxiliary electronics. A numerical model, with Peltier heat, Thompson heat, Joule heat, gap heat leakage, and ceramic covering thermal resistance considered, is built to analyze the performance of the segmented TEG accurately. This design owns reasonable energy output and it is easy to be installed on site.

2. Experimental setup

The experimental setup of the energy harvester to supply power to the gas turbine sensing and monitoring system is presented in Fig. 2. The temperature of the gas turbine surface is as high as 300 °C. The TEG used here is a commercial Bi_2Te_3–PbTe hybrid thermoelectric power module (56 mm × 56 mm) from TECTEG MFR [48], which is optimized for hot side temperatures in the 250–370 °C range. Generally, the body of the gas turbine is covered with a thick thermal isolation layer to improve the energy conversion efficiency. As the TEG module is embedded in the thermal isolation material, two heat pipes with a maximum operating temperature of 200 °C are employed to penetrate the thermal isolation material and dissipate heat from the cold side of the TEG module. The diameter and length of the heat pipe are 10 mm and 152.4 mm, respectively. Ref. [49] announced that, compared with aluminum rod, heat pipe can significantly improve the performance of the TEG module. To implement the device on the gas turbine, it is not practical to use extra device to cool the cold end of the device. Cooling water or fans will make the device burdensome and unreliable, so only natural convection is used here. Two compact and high efficient heat sinks made by ALPHA Company are selected and installed symmetrically at the cold end of the heat pipe. Two 200 W cartridge heater (CIR-20252, OMEGA Engineering) and a temperature controller (CN7800, OMEGA Engineering) are used to control the source temperature during the experiment. Four K-type thermocouples with an error of 0.75% were used to measure the hot & cold side temperatures of the TEG module and the temperature of the heat sink base. Two data acquisitions (DAQs) from National Instruments Inc, NI TB-9214 (with an accuracy of 0.45 K) and NI USB 6008 (with an accuracy of 7.7 mV),

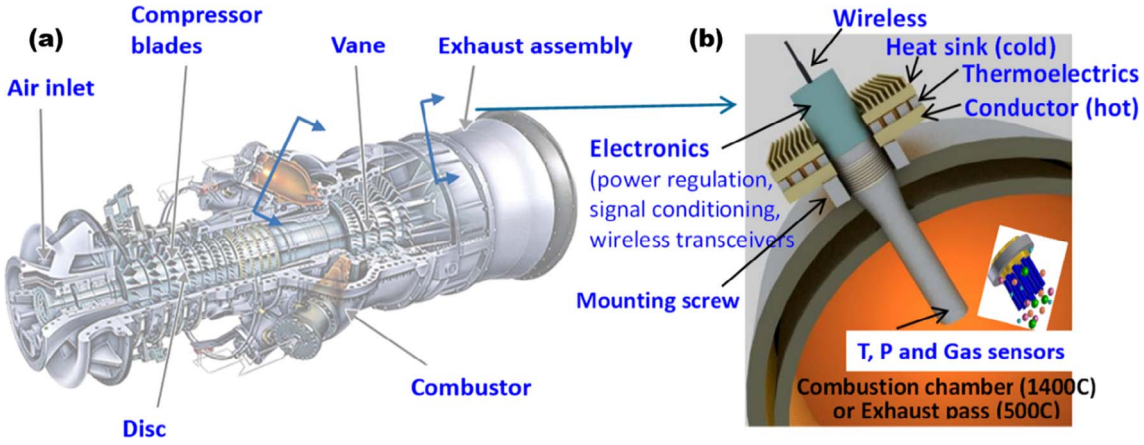

Fig. 1. The concept of using TEG to power the sensing and monitoring system in the gas turbine: (a) a typical gas turbine used for power generation; (b) self-powered temperature, pressure, and gas sensors imbedded in the gas turbine.

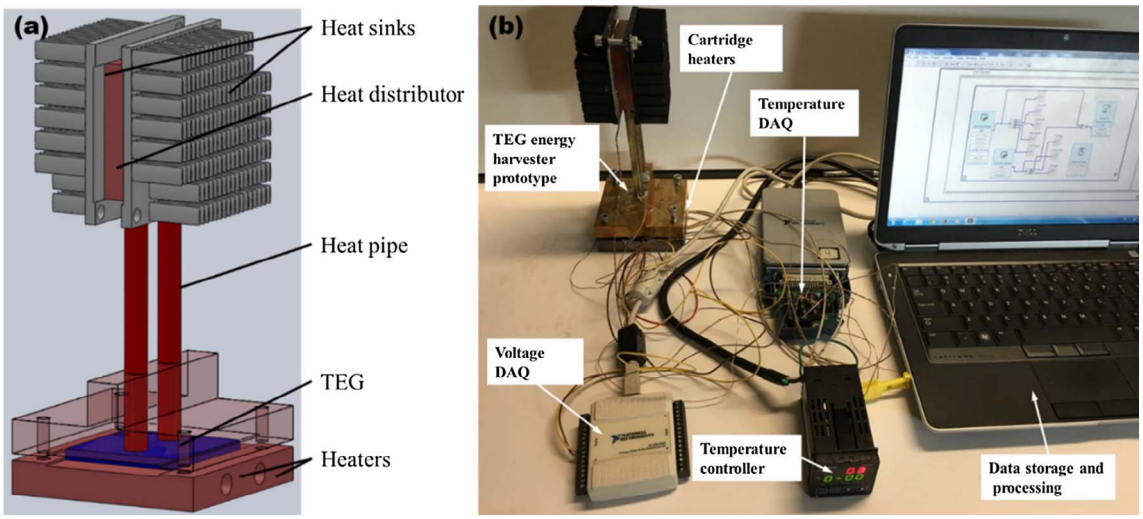

Fig. 2. (a) TEG energy harvester prototype; (b) Experimental setup.

are used to collect the temperature and voltage readings separately. The experiment is carried out in a room with large space and the room temperature is constant at 22.5 °C.

3. Mathematical model

Fig. 3(a) shows the thermal network of the TEG energy harvester prototype. To the best of our knowledge, there are no analytical models which can accurately give the thermal resistance of the heat pipe. Also, the intricate geometry structure of the heat sink introduces extra complexity in the calculation of the convective heat transfer coefficient. Though there are some empirical equations [50,51], they can only be applied to a specific condition and predict the order of the thermal resistance. In this paper, we separate the thermal analysis into several parts, where the TEG module is emphatically studied, while the performance information of heat sink and heat pipe were cited from the datasheet of the products. The model presented here can predict the performance of the segmented TEG module, with Peltier heat, Thompson heat, Joule heat, gap heat leakage, and ceramic covering thermal resistance fully discussed. In the calculation, the properties of the materials are temperature dependent.

The thermal resistances of the thermoelectric materials are temperature dependent. The overall thermal resistances of the P, N-type thermo-element segments are given by

$$RH_{P1} = \frac{1}{A_{P1}}\int_0^{L_{P1}} \frac{1}{k_{P1}}dx,\ RH_{P2} = \frac{1}{A_{P2}}\int_0^{L_{P2}} \frac{1}{k_{P2}}dx \tag{1-1}$$

$$RH_{N1} = \frac{1}{A_{N1}}\int_0^{L_{N1}} \frac{1}{k_{N1}}dx,\ RH_{N2} = \frac{1}{A_{N2}}\int_0^{L_{N2}} \frac{1}{k_{N2}}dx \tag{1-2}$$

Similarly, the thermal resistances of ceramic covering at the hot and cold ends of the segmented TEG are

$$RH_H = \frac{L_H}{k_H A_H}, RH_C = \frac{L_C}{k_C A_C} \tag{2}$$

The gap between the thermo-elements is filled by thermal isolation material, such as air. The energy loss through radiation can be significant in high temperature environment [52]. The thermal resistance of the air filling gap can be calculated by [53]

$$RH_G = 1 \Big/ \left[\frac{k_G A_G}{L_G} + \varepsilon\sigma A_G F_{hc}(T_h^2 + T_c^2)(T_h + T_c)\right] \tag{3}$$

While a segmented TEG has a high efficiency than a single-material-made TEG, the complex geometry causes some new issues, including compatibility problem [23,54], thermal expansion mismatch [55], and contact resistance at the interfaces [56,57]. For our case, the thermal and electrical contact resistances at the interfaces between different material layers are negligible when compared with the resistance of the bulk TEG material [39].

For a thermo-element, the relationships between the cross-section areas are given by

$$A_P = A_{P1} = A_{P2}, A_N = A_{N1} = A_{N2}, A_H = A_C = A_P + A_N + A_G \tag{4}$$

The lengths of the P- and N-type thermo-elements are the same,

$$L = L_{P1} + L_{P2} = L_{N1} + L_{N2} \tag{5}$$

The Fourier heat going through the air gap without passing the thermo-element is

$$q_G = \frac{T_h - T_c}{RH_G} \tag{6}$$

Similarly, the thermal energy entering/leaving the module can be obtained by

$$q_H = \frac{T_H - T_h}{RH_H}, q_C = \frac{T_c - T_C}{RH_C} \tag{7}$$

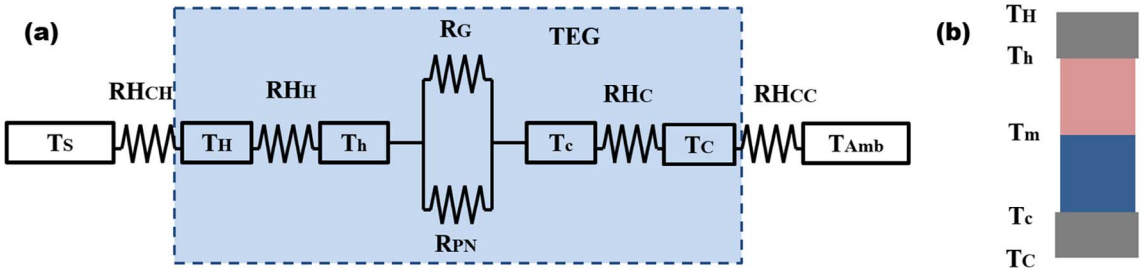

Fig. 3. (a) Thermal network of the energy harvesting system; (b) Segmented thermo-element.

The heat fluxes entering the hot end and leaving the cold end of the thermo-elements are

$$q_h = q_{Nh} + q_{Ph} = (\alpha_{P1}^h - \alpha_{N1}^h) T_h I - k_{N1}^{T_h} A_{N1} \frac{dT_{N1}}{dx}\Big|_{x=L} - k_{P1}^{T_h} A_{P1} \frac{dT_{P1}}{dx}\Big|_{x=L} \tag{8-1}$$

$$q_c = q_{Nc} + q_{Pc} = (\alpha_{P2}^c - \alpha_{N2}^c) T_c I - k_{P2}^{T_c} A_{P2} \frac{dT_{P2}}{dx}\Big|_{x=0} - k_{N2}^{T_c} A_{N2} \frac{dT_{N2}}{dx}\Big|_{x=0} \tag{8-2}$$

where the first term is the Pielter heat and the last two terms are Fourier heat through P- and N- type thermo-elements.

The open circuit voltage of the device caused by Seebeck effect is

$$V = N\left\{\int_{T_c}^{T_{m1}} \alpha_{P2} dT + \int_{T_{m1}}^{T_h} \alpha_{P1} dT - \int_{T_c}^{T_{m2}} \alpha_{N1} dT - \int_{T_{m2}}^{T_h} \alpha_{N2} dT\right\} \tag{9}$$

The electrical resistance of the TEG module is the sum of thermal resistance of all the thermo-elements, thus

$$R_M = N\left[\frac{1}{A_{P2}}\int_0^{L_{P2}} \rho_{P2} dx + \frac{1}{A_{P1}}\int_{L_{P2}}^{L} \rho_{P1} dx + \frac{1}{A_{N2}}\int_0^{L_{N2}} \rho_{N2} dx + \frac{1}{A_{N1}}\int_{L_{N2}}^{L} \rho_{N1} dx\right] \tag{10}$$

When a load resistance connected, the loop current through the thermo-elements is described as

$$I = \frac{V}{R} = \frac{V}{R_L + R_M} \tag{11}$$

And the corresponding power output of the module is

$$P = I^2 R_L = \frac{R_L}{(R_L + R_M)^2} V^2 \tag{12}$$

Combing Eqs. (8-1), (10) and (12) gives the efficiency of the TEG module

$$\eta = \frac{P}{q_h} = \frac{\left[N\left(\sum_1^n \int_0^{L_{Pn}} (\alpha_P \frac{dT}{dx}) dx - \sum_1^n \int_0^{L_{Nn}} (\alpha_N \frac{dT}{dx}) dx\right)\right]^2 R_L}{\left\{R_L + N\left[\sum_0^n \int_0^{L_{Pn}} \left(\frac{\rho_P}{A_P}\right) dx + \sum_0^n \int_0^{L_{Nn}} \left(\frac{\rho_N}{A_N}\right) dx\right]\right\}^2 \left[(\alpha_{P1}^h - \alpha_{N1}^h) T_h I - k_{N1}^h A_{N1} \frac{dT_{N1}}{dx}\Big|_{x=L} - k_{P1}^h A_{P1} \frac{dT_{P1}}{dx}\Big|_{x=L}\right]} \tag{13}$$

An energy balance is achieved at the hot and cold ends of the thermo-elements, the heat flux going through the module comes from the air gap and thermo-elements,

$$q_H = q_h + q_G \tag{14-1}$$

$$q_C = q_c + q_G \tag{14-2}$$

where the heat fluxes going through the thermo-elements are given as

$$q_h = q_{Nh} + q_{Ph} \tag{15-1}$$

$$q_c = q_{Nc} + q_{Pc} \tag{15-2}$$

Substituting Eqs. (6) and (7) into Eq. (14) gives the relationship between the source temperatures (T_H and T_C) and the temperature at the cold and hot ends of the thermo-elements,

$$\frac{T_H - T_h}{RH_H} = q_h + \frac{\Delta T}{RH_G} \tag{16-1}$$

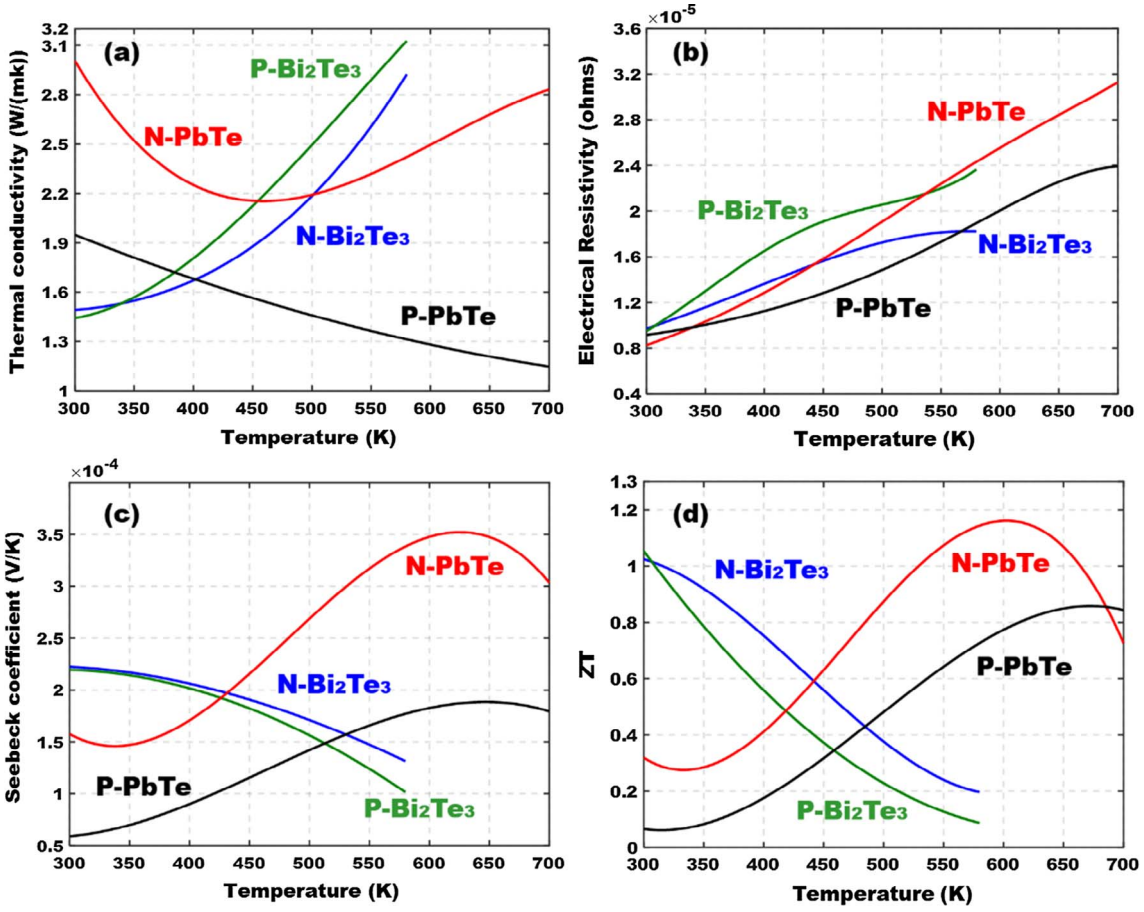

Fig. 4. Properties of the P, N-type thermoelectric materials varying with temperature [60]: (a) Thermal conductivity; (b) Electrical resistivity; (c) Seebeck coefficient; (d) ZT.

$$\frac{T_c - T_C}{RH_C} = q_c + \frac{\Delta T}{RH_G} \tag{16-2}$$

Substituting Eq. (15) into Eq. (16), the cold and hot end temperatures of the thermo-elements are rewritten as

$$T_c = (q_{Pc} + q_{Nc})RH_C + \frac{RH_C}{RH_G}\Delta T + T_C \tag{17}$$

$$T_h = -(q_{Ph} + q_{Nh})RH_H - \frac{RH_C}{RH_G}\Delta T + T_H \tag{18}$$

The thermodynamic governing equation in the thermo-element is given by Domenicali [58],

$$\frac{\partial}{\partial x}\left(k\frac{\partial T}{\partial x}\right) + \rho J^2 - JT\frac{\partial \alpha}{\partial x} = 0 \tag{19}$$

Similar to Eq. (8), the heat flux at the cross-section of the thermo-element is the sum of Peltier heat and Fourier heat

$$q = J\alpha T - k\frac{\partial T}{\partial x} \tag{20}$$

Eq. (20) can be rearranged as [59]

$$\frac{\partial T}{\partial x} = \frac{1}{k}[J\alpha T - q] \tag{21}$$

For this case, $\frac{\partial J}{\partial x} = 0$. Differentiating Eq. (20) on both sides gives

$$\frac{\partial q}{\partial x} = JT\frac{\partial \alpha}{\partial x} + J\alpha\frac{\partial T}{\partial x} - \frac{\partial}{\partial x}\left(k\frac{\partial T}{\partial x}\right) \tag{22}$$

Substituting Eqs. (19) and (20) into Eq. (22), we arrive

$$\frac{\partial q}{\partial x} = \rho J^2\left[1 - \frac{\alpha^2}{\rho k}T\right] - \frac{J\alpha q}{k} \tag{23}$$

Discretizing Eqs. (21) and (23), the temperature and heat flux profiles along the thermo-elements can be explicitly calculated by

$$T_i = T_{i-1} + \frac{(JT_{i-1}\alpha_{i-1} - q_{i-1})}{k_{i-1}}\Delta x_i \tag{24}$$

$$q_i = q_{i-1} + \left[\rho_{i-1}J^2\left(1 - \frac{\alpha_{i-1}^2 T_{i-1}}{\rho_{i-1}k_{i-1}}\right) - \frac{J\alpha_{i-1}}{k_{i-1}}q_{i-1}\right]\Delta x_i \tag{25}$$

In the calculation, the temperatures at the hot (T_h) and cold (T_c) ends of thermo-elements are unknown. The two temperatures are correlated with the temperatures at the hot (T_H) and cold (T_C) ends of the TEG module through Eq. (18), which are measured by the thermocouples. According to the datasheet provided by the TECTEG MFR. corporation, the properties of the P, N-type thermoelectric materials (Fig. 4) are highly temperature dependent [60]. Thus Thompson Effect cannot be neglected in this case. An iterative scheme is carried out to calculate the temperature profiles and other parameters of the TEG module, with the procedures presented in Fig. 5.

4. Results and discussion

The voltage output of a TEG module is positively correlated with the temperature difference. To harvest enough energy for the wireless sensor nodes, a high-temperature drop within the TEG module is desired. Fig. 6(a) shows the voltage output of the prototype for different load resistances with the source temperature increasing from 20 to 325 °C. Limited by the temperature restriction of the heat pipe, the hot side temperature is heated up to a maximum value of 350 °C, with a peak open circuit voltage output of 2.4 V. An even higher open circuit voltage output can be expected with a higher source temperature. The collected data fluctuates slightly with source temperature, which can be reasoned by the hysteresis effect caused by the thermal mass of the system. As depicted in Fig. 6, the numerical result matches very well with the experimental result, showing that the model we developed in the section above can predict the voltage output of the system very well within the whole operation temperature range. As shown in Fig. 6(a), the voltage output of the module does not linearly increase with the source temperature, which can be explained as follows. First, the thermal resistances of the heat pipe and the heat sink vary with the temperature, thus the temperature drop in the TEG module is not linearly correlated with the source temperature. Second, the properties of the thermoelectric materials are temperature dependent, thus the voltage output of the module does not linearly increase with the temperature difference.

The most important parameter to judge the performance of the TEG energy harvester is the power output at the optimum load resistance. As shown in Fig. 6(b), the power output of the TEG module increases significantly with the source temperature. With a load resistance of 1.5 Ω and a source temperature of 325 °C, the prototype can harvest about 0.92 W electrical energy for the sensor nodes embedded in the gas turbine. Different sensor nodes have different requirements for the voltage and power supply. As reported in [27], for a typical sensor node working in the transmission mode, the energy consumption is about 49.3 mW. As the working condition of the gas turbine may change during the operation process, the power output of the TEG module changes accordingly. In addition, the working voltages of the sensors are different. To provide stable and continuous power and voltage supply for the sensing and monitoring system, integrated energy management circuits with low energy consumption should be designed. The total power requirement for the electrical management circuit and wireless communication components is less than 1.0 W [49]. The prototype presented above can supply more than enough power for the sensors and auxiliary electronics.

As shown in Fig. 7(a), the cold side temperature of the TEG module and the temperature of the heat sink base increase with the source temperature. For different load resistances, the experimental results are highly repeatable, because the amount of energy converted into electricity is relatively small. When the hot side temperature is 325 °C, the temperature drop in the TEG module is about 42 °C, while the temperature drops in the heat pipe and the heat sink are as high as 75 and 120 °C, respectively.

The peak efficiency of the TEG module is determined by ZT value and temperature drop in the thermo-elements. We calculate the efficiency of the TEG module based on the modeling results with different load resistance (Fig. 7(b)). With a load resistance of 1.5 Ω, the

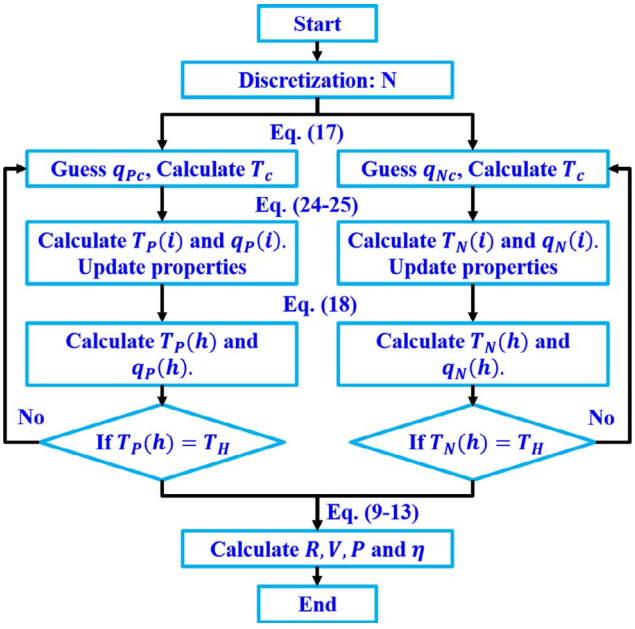

Fig. 5. The iteration scheme for the TEG model.

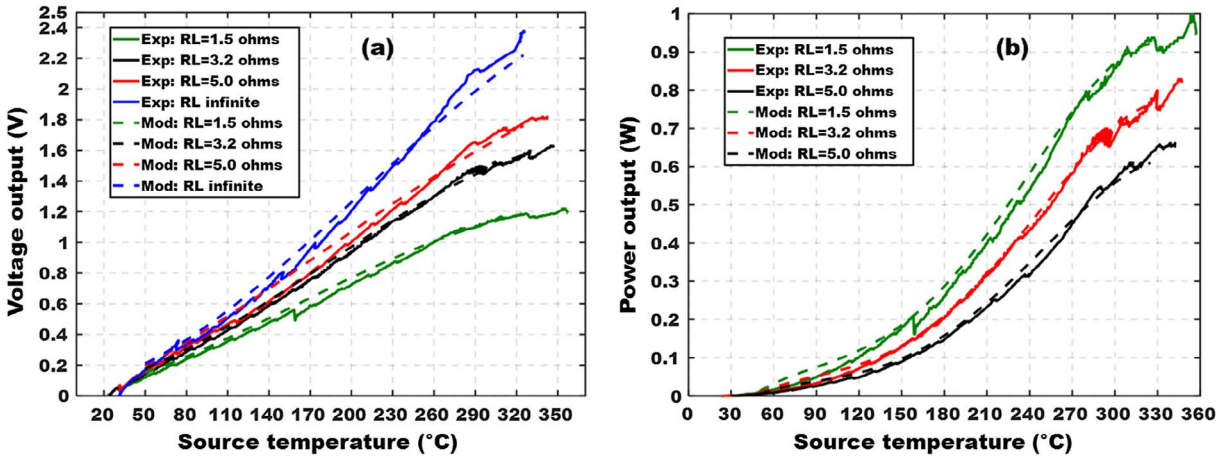

Fig. 6. The comparison of the experimental and modeling results: (a) Voltage output and (b) power output of the of the thermoelectric energy harvester prototype.

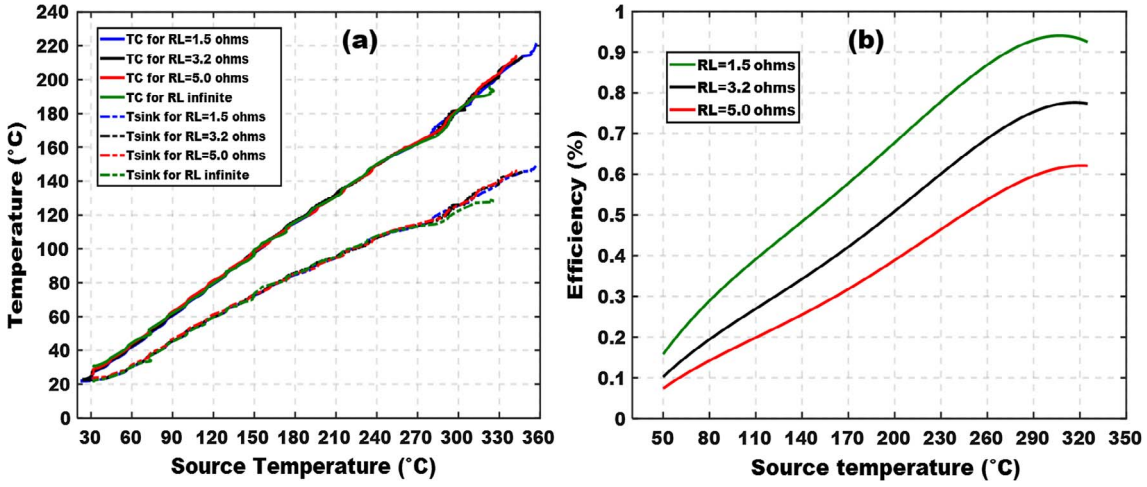

Fig. 7. (a) T_C and T_{sink} change versus the source temperature; (b) The efficiency of the TEG module.

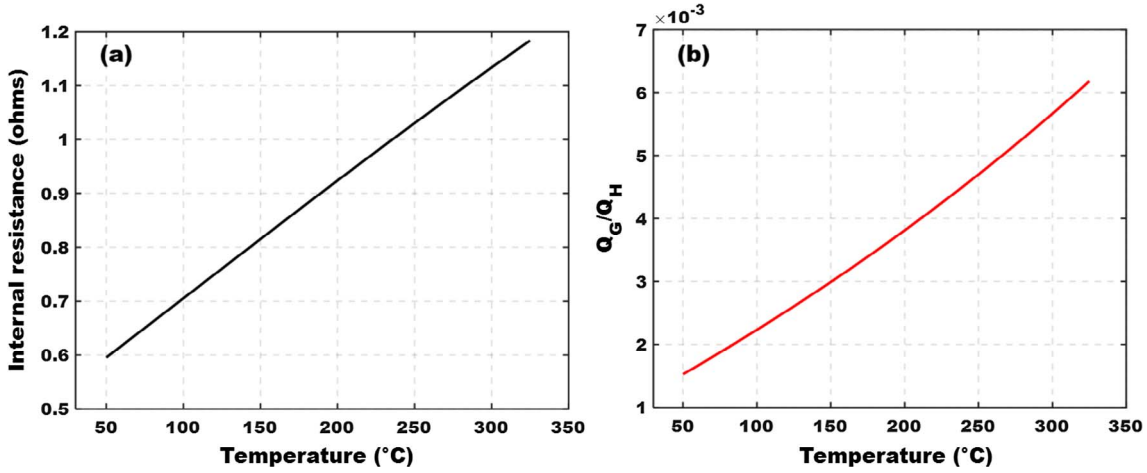

Fig. 8. (a) Internal resistance and (b) radiation heat leakage varying with source temperature.

efficiency increases with source temperature and reaches to a peak value of 0.94%, which is relatively low for a segmented TEG. This low efficiency is reasoned as follows. First, natural convection is less efficient than other cooling methods. Thus the thermal resistance of the heat sink is relatively high. Second, several thermal contact layers exist in the prototype, further increasing the thermal resistance of thermal network. Though the source temperature is high (325 °C), the temperature drop within the thermo-element is relatively small (~45 °C), which is validated by the calculated temperature profile presented in Fig. 7(a). There is still some room further improving the performance of the energy harvester through optimization of the thermal network. The convenient ways to increase the power output and efficiency includes adopting heat sink and heat pipe with better performance and using forced convection. However, these methods improve the performance of the energy harvester at the cost of system geometry size and reliability. Improving the contact quality is a more practical way to improve

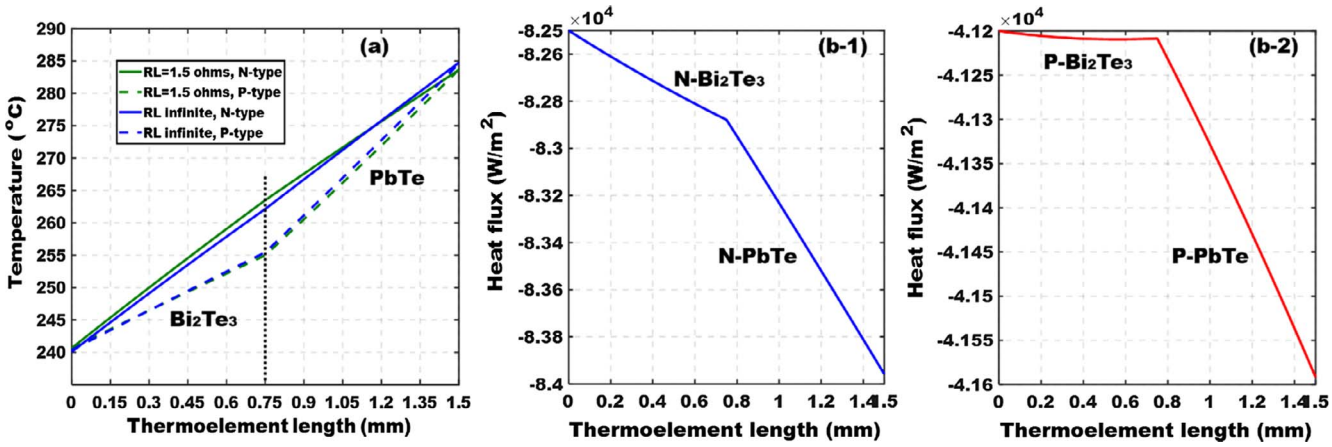

Fig. 9. (a) The calculated temperature profiles in the thermo-elements; (b) Heat fluxes through the thermo-elements with R_L = 1.5 Ω.

the system performance.

Note that the TEG achieves the peak power output when the load resistance equals to the internal resistance of the TEG module. As we can see in Fig. 8(a), the internal resistance of the TEG module almost doubles with the source temperature changing from 50 °C to 325 °C. Since the optimum load resistance of the TEG is temperature dependent, an electronic power tracking system can be developed to maximize the power output of the module. Generally, the radiative heat transfer was neglected in the thermal analysis of TEG module, especially when the temperature difference is small [41]. However, for TEG module working at high temperature, the radiative heat leakage can be significant. As is observed in Fig. 8(b), the heat leakage through the line spacing increases with the source temperature, accounting for 0.61% of the total heat flow through the device when the source temperature is 325 °C.

In the TEG module, as a small proportion of thermal energy is converted into electricity and properties of the materials vary with temperature, the temperature in the TEG module is not linearly distributed along the thermo-element length, as presented in Fig. 9(a). With load resistance changing from infinite to 1.5 Ω, the nonlinearity of the temperature profile increases, because larger proportion of thermal energy is converted into electricity. This phenomenon is more obviously observed in the N-type thermo-element. Note that, even when the source temperature is the same, the hot and code side temperatures of the thermo-elements will vary with the load resistance change. The energy conversion process is illustrated clearly in Fig. 9(b), as the heat fluxes decrease along the thermal elements. According to the energy conservation law, the “disappeared” thermal energy is converted to electrical energy. An insight observation of the thermal fluxes along the thermo-element finds that PbTe segment has higher conversion efficiency than Bi2Te3 at this operation temperature range. P-type Bi_2Te_3 has very low efficiency, as the compatibility factors of P-type PbTe and Bi_2Te_3 do not match well in this temperature range. Segmented TEG module with optimized design is desired to enhance the energy conversion efficiency.

5. Conclusions

In this paper, a compact and reliable segmented TEG energy harvester is designed to power wireless sensor nodes in the gas turbine, providing continuous data for the sensing and monitoring system. After a detailed analysis of the TEG energy system, we can safely conclude that

(1) With the hot side of the TEG heated up to 325 °C, the module has a peak open circuit voltage output of 2.4 V and a power output of ~0.92 W, which is more than enough to power quite a few wireless sensors in the gas turbine.
(2) An accurate model to analyze a segmented TEG module is developed, with Peltier heat, Thompson heat, Joule heat, gap heat leakage, and ceramic covering thermal resistance are considered. The resistance of the TEG module almost doubles with the source temperature changing from 50 °C to 325 °C. Meanwhile, the radiation heat leakage increases significantly with the increase in source temperature.
(3) The temperature distribution along the thermo-element is nonlinear, as the properties of the thermoelectric materials are temperature dependent and the energy conversion process exists in the thermoelectric materials. The energy conversion process is observed clearly by noticing the decrease of heat flux along the thermo-element length.
(4) The energy conversion efficiency of the prototype is about 0.94% with a source temperature of 325 °C and a load resistance of 1.5 Ω. As only natural convection is used to cool the heat sink, the thermal resistance of the heat sink is high, making the efficiency of the TEG relatively low. There is a tradeoff between higher energy output and smaller energy harvester size.

Acknowledgement

The authors wish to thank the support of US National Science Foundation via Grant #1529842 and #1335384.

References

[1] Scherrer H, Scherrer S, Rowe D. Thermoelectric Handbook-Macro to Nano ed. Rowe, DM: Taylor & Francis; 2006.
[2] Bell LE. Cooling, heating, generating power, and recovering waste heat with thermoelectric systems. Science 2008;321:1457–61.
[3] Tritt TM, Subramanian MA. Thermoelectric materials, phenomena, and applications: a bird's eye view. Mrs Bull 2006;31:188–94.
[4] Hicks LD, Dresselhaus MS. Thermoelectric figure of merit of a one-dimensional conductor. Phys Rev B 1993;47:16631–4.
[5] Hicks LD, Dresselhaus MS. Effect of quantum-well structures on the thermoelectric figure of merit. Phys Rev B 1993;47:12727–31.
[6] Snyder GJ, Toberer ES. Complex thermoelectric materials. Nat Mater 2008;7:105–14.
[7] Tan GJ, Zhao LD, Kanatzidis MG. Rationally designing high-performance bulk thermoelectric materials. Chem Rev 2016;116:12123–49.
[8] Harman TC, Walsh MP, Laforge BE, Turner GW. Nanostructured thermoelectric materials. J Electron Mater 2005;34:L19–22.
[9] Smith CJW, Cahill JS, Nuhoglu A. Macro to nano: scaling effects of Bi_2Te_3 thermoelectric generators for applications in space. PAM Rev: Energy Sci Technol 2016;3:86–99.
[10] Zhao LD, Lo SH, Zhang YS, Sun H, Tan GJ, Uher C, et al. Ultralow thermal conductivity and high thermoelectric figure of merit in SnSe crystals. Nature 2014;508:373. +.
[11] Tan GJ, Shi FY, Hao SQ, Chi H, Zhao LD, Uher C, et al. Codoping in SnTe: enhancement of thermoelectric performance through synergy of resonance levels and band convergence. J Am Chem Soc 2015;137:5100–12.

[12] Yu B, Zebarjadi M, Wang H, Lukas K, Wang HZ, Wang DZ, et al. Enhancement of thermoelectric properties by modulation-doping in silicon germanium alloy nanocomposites. Nano Lett 2012;12:2077–82.
[13] Zhao LD, Wu HJ, Hao SQ, Wu CI, Zhou XY, Biswas K, et al. All-scale hierarchical thermoelectrics: MgTe in PbTe facilitates valence band convergence and suppresses bipolar thermal transport for high performance. Energ Environ Sci 2013;6:3346–55.
[14] He JQ, Sootsman JR, Girard SN, Zheng JC, Wen JG, Zhu YM, et al. On the origin of increased phonon scattering in nanostructured PbTe based thermoelectric materials. J Am Chem Soc 2010;132:8669–75.
[15] Biswas K, He JQ, Zhang QC, Wang GY, Uher C, Dravid VP, et al. Strained endotaxial nanostructures with high thermoelectric figure of merit. Nat Chem 2011;3:160–6.
[16] Zhao LD, Hao SQ, Lo SH, Wu CI, Zhou XY, Lee Y, et al. High thermoelectric performance via hierarchical compositionally alloyed nanostructures. J Am Chem Soc 2013;135:7364–70.
[17] Venkatasubramanian R, Siivola E, Colpitts T, O'Quinn B. Thin-film thermoelectric devices with high room-temperature figures of merit. Nature 2001;413:597–602.
[18] Hudak NS, Amatucci GG. Small-scale energy harvesting through thermoelectric, vibration, and radiofrequency power conversion. J Appl Phys 2008;103.
[19] Snyder GJ. Small thermoelectric generators. Electrochem Soc Interf 2008;17:54.
[20] Kraemer D, Poudel B, Feng HP, Caylor JC, Yu B, Yan X, et al. High-performance flat-panel solar thermoelectric generators with high thermal concentration. Nat Mater 2011;10:532–8.
[21] Hadjistassou C, Kyriakides E, Georgiou J. Designing high efficiency segmented thermoelectric generators. Energ Convers Manage 2013;66:165–72.
[22] Ming T, Wu Y, Peng C, Tao Y. Thermal analysis on a segmented thermoelectric generator. Energy 2015;80:388–99.
[23] Snyder GJ, Caillat T. Using the compatibility factor to design high efficiency segmented thermoelectric generators. Thermoelect Mater 2003-Res Appl 2004;793:37–42.
[24] Longtin JP, Zuo L, Hwang D, Fu GS, Tewolde M, Chen YK, et al. Fabrication of thermoelectric devices using thermal spray: application to vehicle exhaust systems. J Therm Spray Techn 2013;22:577–87.
[25] Hsu CT, Huang GY, Chu HS, Yu B, Yao DJ. Experiments and simulations on low-temperature waste heat harvesting system by thermoelectric power generators. Appl Energy 2011;88:1291–7.
[26] Yazawa K, Koh YR, Shakouri A. Optimization of thermoelectric topping combined steam turbine cycles for energy economy. Appl Energy 2013;109:1–9.
[27] Samson D, Kluge M, Becker T, Schmid U. Energy harvesting for autonomous wireless sensor nodes in aircraft. Procedia Eng 2010;5:1160–3.
[28] Huesgen T, Woias P, Kockmann N. Design and fabrication of MEMS thermoelectric generators with high temperature efficiency. Sensor Actuat A – Phys 2008;145:423–9.
[29] Starner T, Paradiso JA. Human generated power for mobile electronics. Low Power Electron Des 2004;45:1–35.
[30] Snyder GJ, Lim JR, Huang CK, Fleurial JP. Thermoelectric microdevice fabricated by a MEMS-like electrochemical process. Nat Mater 2003;2:528–31.
[31] Paradiso JA, Starner T. Energy scavenging for mobile and wireless electronics. IEEE Pervasive Comput 2005;4:18–27.
[32] Clayton DA, Willems RA. Design Considerations for Wireless Sensor Networks in Nuclear Power Applications. Oak Ridge National Laboratory (ORNL); 2015.
[33] Kuramitsu M, Redondo JM, Noriega G. Measurements of anisotropy, thermoelectric behaviour and multi-fractal aspects of FeSi and of complex custom made TE materials. In: Twenty-Second international conference on thermoelectrics, proceedings Ict '03; 2003. p. 541–5.
[34] Kim SJ, We JH, Cho BJ. A wearable thermoelectric generator fabricated on a glass fabric. Energ Environ Sci 2014;7:1959–65.
[35] Cook BW, Lanzisera S, Pister KSJ. SoC issues for RF smart dust. P IEEE 2006;94:1177–96.
[36] Warneke B, Last M, Liebowitz B, Pister KSJ. Smart dust: communicating with a cubic-millimeter computer. Computer 2001;34:44. +.
[37] Wang ZY, Leonov V, Fiorini P, Van Hoof C. Realization of a wearable miniaturized thermoelectric generator for human body applications. Sensor Actuat A – Phys 2009;156:95–102.
[38] Stark I. Invited talk: thermal energy harvesting with Thermo Life. International Workshop on Wearable and Implantable Body Sensor Networks (BSN'06). IEEE; 2006. p. 19–22.
[39] Wu Y, Zuo L, Chen J, Klein JA. A model to analyze the device level performance of thermoelectric generator. Energy 2016;115:591–603.
[40] Freunek M, Muller M, Ungan T, Walker W, Reindl LM. New physical model for thermoelectric generators. J Electron Mater 2009;38:1214–20.
[41] Chen JC, Yan ZJ, Wu LQ. The influence of Thomson effect on the maximum power output and maximum efficiency of a thermoelectric generator. J Appl Phys 1996;79:8823–8.
[42] Chen M, Rosendahl LA, Condra T. A three-dimensional numerical model of thermoelectric generators in fluid power systems. Int J Heat Mass Tran 2011;54:345–55.
[43] Jang JY, Tsai YC, Wu CW. A study of 3-D numerical simulation and comparison with experimental results on turbulent flow of venting flue gas using thermoelectric generator modules and plate fin heat sink. Energy 2013;53:270–81.
[44] Kumar S, Heister SD, Xu XF, Salvador JR, Meisner GP. Thermoelectric generators for automotive waste heat recovery systems Part I: Numerical modeling and baseline model analysis. J Electron Mater 2013;42:665–74.
[45] Meng FK, Chen LG, Sun FR. A numerical model and comparative investigation of a thermoelectric generator with multi-irreversibilities. Energy 2011;36:3513–22.
[46] Han J-C, Datta S, Ekkad S. Gas turbine heat transfer and cooling technology. 2nd ed. Boca Raton, FL: CRC Press/Taylor & Francis; 2013.
[47] Padture NP, Gell M, Jordan EH. Materials science – thermal barrier coatings for gas-turbine engine applications. Science 2002;296:280–4.
[48] T. MFR. Hybrid Thermoelectric Power Modules PbTe-BiTe; 2016.
[49] Chen J, Zuo L, Wu YJ, Klein J. Modeling, experiments and optimization of an on-pipe thermoelectric generator. Energ Convers Manage 2016;122:298–309.
[50] Bejan A. Convection heat transfer, 4th ed.
[51] Reay DA, Kew PA, McGlen RJ, Books24x7 Inc., Heat pipes theory, design and applications, sixth edition. 6th ed. Butterworth-Heinemann, Kidlington, Oxford, UK; Waltham, MA; 2014.
[52] Ouyang ZL, Li DW. Modelling of segmented high-performance thermoelectric generators with effects of thermal radiation, electrical and thermal contact resistances. Sci Rep-UK 2016;6.
[53] Bergman TL, Incropera FP. Fundamentals of heat and mass transfer. 7th ed. Hoboken, NJ: John Wiley; 2011.
[54] Snyder GJ, Ursell TS. Thermoelectric efficiency and compatibility. Phys Rev Lett 2003;91.
[55] Wu YJ, Ming TZ, Li XH, Pan T, Peng KY, Luo XB. Numerical simulations on the temperature gradient and thermal stress of a thermoelectric power generator. Energ Convers Manage 2014;88:915–27.
[56] Bjork R. The universal influence of contact resistance on the efficiency of a thermoelectric generator. J Electron Mater 2015;44:2869–76.
[57] Wu YJ, Zuo L, Chen J, Klein JA. A model to analyze the device level performance of thermoelectric generator. Energy 2016;115:591–603.
[58] Domenicali CA. Irreversible thermodynamics of thermoelectric effects in inhomogeneous, anisotropic media. Phys. Rev. 1953;92:877–81.
[59] Mahan GD. Inhomogeneous thermoelectrics. J Appl Phys 1991;70:4551–4.
[60] T. MFR. Thermoelectric Generator Power Bulk Materials BiTe, PbTe; 2016.